

# Evaporation based micro pump integrated into a scanning force microscope probe

F. Heuck<sup>c,\*</sup>, T. Hug<sup>c</sup>, T. Akiyama<sup>c</sup>, P.L.T.M. Frederix<sup>b</sup>, A. Engel<sup>b</sup>, A. Meister<sup>a</sup>,  
H. Heinzelmann<sup>a</sup>, N.F. de Rooij<sup>c</sup>, U. Staufer<sup>c</sup>

<sup>a</sup> CSEM SA, 2002 Neuchatel, Switzerland

<sup>b</sup> M.E. Mueller Institute, University of Basel, 4056 Basel, Switzerland

<sup>c</sup> Institute of Microtechnology, University of Neuchatel, 2002 Neuchatel, Switzerland

## Abstract

A micro pump was integrated into a scanning force microscope probe for circulating liquid through its hollow cantilever and tip. The interior cross section of the cantilever was  $2.25 \mu\text{m} \times 3.75 \mu\text{m}$ . All fluidic parts were made of  $\text{SiO}_2$ , while the tip apex was made of  $\text{Si}_3\text{N}_4$ . The key fabrication techniques were silicon wafer bonding and wet-oxidation. The pumping mechanism was relying on the enhanced evaporation at an enlarged water/air interface at the exit of the microchannel. Capillary forces continuously wetted this interfacial area, thus drawing the liquid through the system. At room temperature, a pump rate of  $11 \text{ pl s}^{-1}$  was experimentally evaluated. The observed temperature dependence of the pump rate could be qualitatively understood by a plain model calculation.

*Keywords:* Evaporation driven micro pump; Scanning force microscope; Microfabrication

## 1. Introduction

This work combines two fields of research: micro fluidics and scanning force microscopy (SFM). Compared to other mechanisms used in micro fluidics [1], the concept of evaporation driven pumps enables low and continuous flow rates. Its main application is currently in lab-on-a-chip research [2], where it is used for e.g. sample concentration [3] or chromatography [4]. A combination of microfluidic with micromechanical structures was used e.g. for weighing biomolecules [5]. A solution of the analyte was pumped through a channel inside an oscillating cantilever, which changed its resonance frequency as function of the liquid mass. A first solution for a combination of pump and an SFM-probe was presented by Hug et al. [6]. The present approach takes up on that work aiming at a scanning ion pipette with fluidic

capabilities. It is meant to locally administer bioactive solutions and to detect structural changes induced by this in cell membranes.

## 2. Theory

This section briefly introduces the theoretical background of the pumping mechanism. A more detailed description can be found in [1]. A sketch of the SFM-probe configuration is schematically shown in Fig. 1a. The hydrophilic  $\text{SiO}_2$  fluidic system is filled from the reservoir with water by capillary force. In the evaporation cell, water evaporates and diffuses through an opening in the chip into the lab. Thus a vapor pressure profile is established ranging from the saturation pressure at the water/air interface to the level given by the humidity in the lab at the surface of the chip. All diffusion losses are replaced by the capillary force drawing additional water through the fluidic system. An  $x$ -coordinate is defined having its origin at the water/air

\* Corresponding author. Tel.: +41 32 720 5305.

E-mail address: friedjof.heuck@unine.ch (F. Heuck).

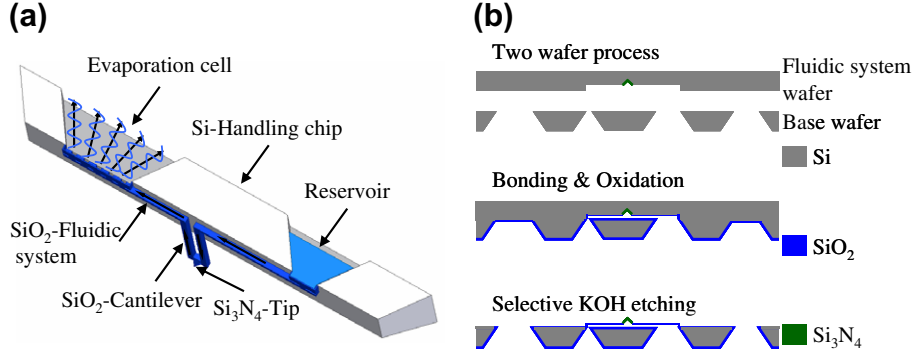


Fig. 1. (a) Sketch of a SFM-probe with an integrated evaporation cell. The reservoir is filled with water. The evaporated water in the evaporation cell induces pumping through the fluidic system. (b) Simplified process flow for the integration of the micro pump into the SFM-probe.

interface and pointing outward, perpendicular to the later. Since diffusion of water vapor is the limiting force of the pump, Fick's first law defines the evaporation rate  $N_E$  [ $\text{mol m}^{-2} \text{s}^{-1}$ ] by

$$N_E = \frac{D}{RT} \left. \frac{\partial p_V}{\partial x} \right|_{x=x_0}, \quad (1)$$

where  $D$  [ $\text{m}^2 \text{s}^{-1}$ ],  $p_V$  [ $\text{N m}^{-2}$ ] and  $R$  [ $\text{J mol}^{-1} \text{K}^{-1}$ ] denote the diffusion constant, the vapor pressure of water and the ideal gas constant, respectively [7]. It is assumed that the temperature  $T$  [K] is constant also at the water/air interface; i.e. the heat loss due to evaporation is compensated. In order to evaluate the pump rate  $P_R$  [ $\text{m}^3 \text{s}^{-1}$ ], the properties of the evaporation cell and of water must be considered:

$$P_R = A_E \frac{M}{\rho_1} N_E = A_E \frac{M}{\rho_1} \frac{D}{RT} \left. \frac{\partial p_V}{\partial x} \right|_{x=x_0}, \quad (2)$$

where  $A_E$  [ $\text{m}^2$ ],  $M$  [ $\text{kg mol}^{-1}$ ] and  $\rho_1$  [ $\text{kg m}^{-3}$ ] denote the area of the water/air interface in the evaporation cell, the molecular weight and the density of water, respectively. In this work the influence of the temperature on the pump rate  $P_R$  was investigated. The temperature has a minor influence on the liquid density  $\rho_1$  [8]. The gradient of the vapor pressure profile  $\partial p_V / \partial x$  has to take the pyramidal geometry of the space in the evaporation cell above the water/air interface into account. In the following case this value is numerically deduced. The temperature dependency of the saturated water vapor at the water/air interface can be described by the Clausius–Clapeyron–equation although numerical values found in [8] were used for a more accurate modelling. Gates et al. investigated the diffusion constant of water vapor  $D$  which they found to depend linearly on the temperature [9].

### 3. Probe design and fabrication results

A simplified process flow for integrating the micro pump into the SFM-probe is described in Fig. 1b, details are given in [6]. The fabrication was based on a two wafer process. The 390  $\mu\text{m}$  thick “fluidic system wafer” contained

a deep reactive ion etched (DRIE) outline of the fluidic system, compensation structures for a later KOH etching step, and a molded  $\text{Si}_3\text{N}_4$  tip. The bottom of the evaporation cell was equipped with an array of narrow, open cavities to wick the liquid away from the exit of the capillary and to increase the liquid–air interface. The also 390  $\mu\text{m}$  thick “base wafer” defined the outer shape of the SFM-probes and provided two through wafer connections per chip to access the fluidic system.

For assembling the two wafers were aligned such that the small openings of the through wafer connections in the base fitted the fluidic system. This sandwich was then wet thermally oxidized by which it was fused and the proper fluidic components were formed by the  $\text{SiO}_2$  film, which grew even at the far end of the channel. Within a certain range the resonance frequency and spring constant of the cantilever could be adjusted by the initial DRIE depth and the thickness of the  $\text{SiO}_2$  film.

To release the cantilever and to have full optical access to the fluidic system, the bonded wafers were etched in KOH from the side of the fluidic system wafer, selectively removing Si against  $\text{SiO}_2$ . Fig. 2a and b present scanning electron microscope images from the sample side of the 155  $\mu\text{m}$  long cantilever and its cross section with interior dimensions of 2.25  $\mu\text{m} \times 3.75 \mu\text{m}$ . The final feature, an opening in the tip has not yet been included and will most likely have to be machined by a focused ion beam.

### 4. Experiments

The suitability of the device for SFM was demonstrated by imaging a fixed and dried *Escherichia coli* bacteria shown in Fig. 2c.

For evaluating the pump, an inverted fluorescence microscope was equipped with CCD camera and a resistively heated, massive aluminum sample holder onto which the device was mounted. The temperature was measured with a thermocouple next to the device. The set-up was covered by an opaque box to ensure light tightness and stable airflow conditions. The device was operated with deionized water into which  $5.7 \times 10^{12}$  spheres  $\text{l}^{-1}$  of 0.2  $\mu\text{m}$

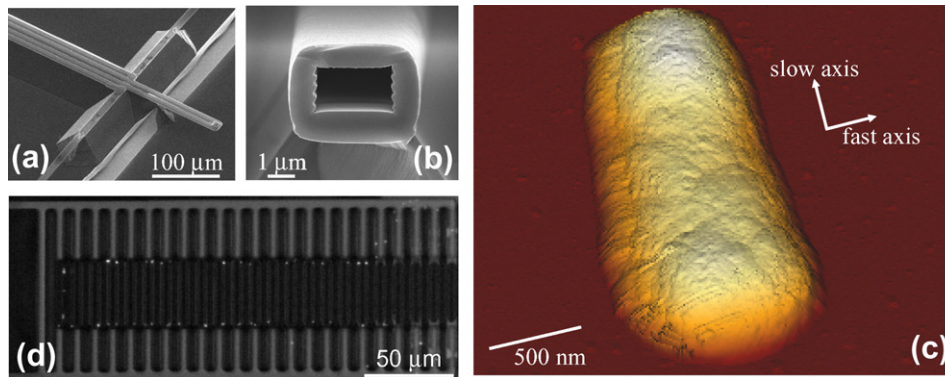


Fig. 2. Scanning electron microscope image from the sample side: (a) cantilever and (b) cross section of a cleaved cantilever. (c) Scanning force microscope image of a fixed and dried *E. coli* bacteria obtained by the SFM-probe. The z-datascale is 550 nm. (d) Optical microscope image of an evaporation cell containing micro spheres, seen from the sample side.

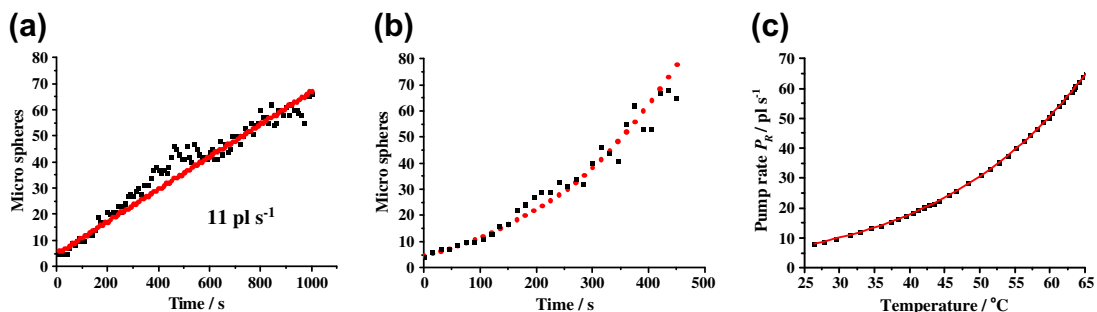


Fig. 3. (a) Accumulation of micro spheres in the evaporation cell at 25 °C. (b) Accumulation of micro spheres in the evaporation cell at increasing temperature. In (a) and (b) the measurement data and the model values are represented by the squares and the dots, respectively. (c) The pump rate  $P_R$  versus the temperature deduced from (b) and the Arrhenius characteristic are represented by the squares and the line, respectively.

diameter fluorescently labeled microspheres (Fluoresbrite, Polyscience) were ultrasonically suspended. The pump rate  $P_R$  was deduced from the accumulation of the spheres in the evaporation cell, which in contrast to the water could not evaporate. Fig. 2d depicts an optical microscope image of the evaporation cell showing microspheres (white dots) seen from the sample side. The distribution of these dots in a straight line indicated that the evaporation area was reduced to the cross section of the capillaries. The capillary force exerted by the top opened cavities in the middle of the evaporation cell was not strong enough to overcome the hydraulic resistance of the fluidic system.

To verify the correctness of this measuring method a control experiment was conducted. All parameters were kept constant; hence a constant pump rate and therefore a linear increase in the amount of particles in the evaporation cell was expected and indeed observed as shown in Fig. 3a. A pump rate of  $11 \text{ pl s}^{-1}$  at 25 °C was deduced.

In a further experiment the dependency of the pump rate  $P_R$  on the temperature  $T$  was investigated. Fig. 3b shows the superposition of the temperature increase and the accumulation of micro spheres in the evaporation cell. The measurement data (squares) was in good agreement with the model values (dots) based on Eq. (2). From this figure the temperature  $T$  dependency of the pump rate  $P_R$  was

deduced as shown in Fig. 3c. The pump rate  $P_R$  showed a Arrhenius characteristics. The geometry dependent pre-exponential factor was  $63 \text{ ml s}^{-1}$  and the enthalpy of vaporization 45 kJ/mol. This value compared well with the tabulated value for water [45.1 kJ/mol (at 0 °C) and 42.5 kJ/mol (at 60 °C)] considering the relatively large experimental error in our measuring method.

## 5. Summary

An evaporation driven micro pump was integrated into an SFM probe. This pump was used to draw liquid through the hollow cantilever of the SFM probe, which had a cross section of  $2.25 \mu\text{m} \times 3.75 \mu\text{m}$ . A pump rate of  $11 \text{ pl s}^{-1}$  @ 25 °C was measured and its temperature dependence was qualitatively investigated. The complete probe was successfully used for imaging a biological sample.

## Acknowledgements

Financial support by NCCR Nanoscale Science of the Swiss National Science Foundation and the Republic and Canton de Neuchatel are acknowledged. The author would like to thank the technical staff of Comlab, the

joint IMT-CSEM clean room facility as well as M. Page and C. Dantier from Basilea Pharmaceuticals (Basel, Switzerland) for the preparation of the *E. coli* bacteria.

## References

- [1] V. Namasivayam, R.G. Larson, D.T. Burke, M.A. Burns, J. Micro-mech. Microeng. 13 (2003) 261–271.
- [2] M. Zimmermann, S. Bentley, H. Schmid, P. Hunziker, E. Delamarche, Lab Chip 5 (2005) 1355–1359.
- [3] G.M. Walker, D.J. Beebe, Lab Chip 2 (2002) 57–61.
- [4] N. Goedecke, J. Eijkel, A. Manz, Lab Chip 2 (2002) 219–223.
- [5] T.P. Burg, M. Godin, S.M. Knudsen, W. Shen, G. Carlson, J.S. Foster, K. Babcock, S.R. Manalis, Nature 446 (2007) 1066–1069.
- [6] T.S. Hug, N.F. deRooij, U. Staufer, Microfluid. Nanofluid. 2 (2006) 117–124.
- [7] R. Bird, W. Stewart, E. Lightfoot, Transport Phenomena, Wiley and Sons, 1960.
- [8] R.C. Weast, M.J. Astle, W.H. Beyer, CRC Handbook of Chemistry, 68th ed., CRC Press, 1988.
- [9] D.M. Gates, Biophysical Ecology, Springer, 1980.